Wall slip in polymer melts

1997 J. Phys.: Condens. Matter 9 7719

(http://iopscience.iop.org/0953-8984/9/37/006)

J. Phys.: Condens. Matter **9** (1997) 7719–7740. Printed in the UK PII: S0953-8984(97)82229-1

Wall slip in polymer melts

L Léger, H Hervet, G Massey and E Durliat

Laboratoire de Physique de la Matière Condensée, URA CNRS 792, Collège de France, 11 Place Marcelin-Berthelot, 75231 Paris Cédex 05, France

Received 25 February 1997

Abstract. We present a review of the recent characterizations of the flow behaviour of high-molecular-weight polymer melts, with special emphasis on situations in which slip at the wall appears. These characterizations are based on direct measurements of the local velocity of the fluid, in the immediate vicinity of the solid wall, through near-field velocimetry techniques. The results demonstrate the importance of polymer molecules anchored on the solid surface, either by strong adsorption or by chemical grafting, and entangled with the bulk polymer, to produce a strong friction at low shear rates and to lead to a shear rate threshold above which strong slip at the wall and low friction develop. The evolution of the shear rate threshold and of the flow characteristics (the length of the extrapolation of the velocity profile to zero, the critical slip velocity for the onset of strong slip, ...) with the molecular parameters of the system (the molecular weights of the bulk and surface chains, and the surface density of anchored chains) is analysed and compared with the predictions of recent theoretical models.

1. Introduction

Many methods of transformation of polymer materials imply steps in which the molten polymer flow is limited by solid surfaces. This is the case, for example, in injection moulding or in the die of an extrusion machine. The quality of the final product is highly sensitive to the flow characteristics, especially to the boundary condition for the velocity at the polymer–wall interface. This is because the stress experienced by the molecules close to the interface is proportional to the local velocity gradient. Under large enough shear stresses these chains can deform, and, if they cannot come back to their equilibrium conformation before solidification, some frozen stresses remain in the final material. For example, in extrusion, defects and instabilities in the shape of the extrudate [1] are known to appear when the interfacial stress reaches a given level which depends on the molecular characteristics of the polymer, the nature of the solid, and the shape of the die.

It has been suspected for a long time that high-molecular-weight polymers, because of their viscoelastic properties (they can display a solid-like or a liquid-like mechanical response depending upon the frequency of the mechanical solicitation), could exhibit a non-zero boundary condition for the flow velocity at the solid wall, or wall slip, contrary to what is usual in simple liquids. A number of investigations have thus attempted to characterize wall slip in polymer systems, first through rheological macroscopic characteristics such as pressure drop as a function of flow rate, for various flow geometries [2–8], and then by trying to characterize the flow behaviour as a function of the thickness of the liquid [9, 10], or determining the velocity gradient by the use of tracer particles or by velocimetry [11, 12]. More recently, direct measurements of the local velocity in the immediate vicinity of the wall (within 100 nm of the wall) [13–15] have appeared. At the same time, several

0953-8984/97/377719+22$19.50

attempts have been made to model flows with slip, and to relate the onset of strong slip to the molecular characteristics of the polymer [16–23]. This is of obvious practical importance, as instabilities in extrusion processes and extrudate defects have been related to the onset of flow with slip boundary conditions [1, 24, 25].

The macroscopic investigations show that the appearance of wall slip depends on the nature of the polymer and surface under investigation. For many cases a limiting shear rate has to be reached before slip can be macroscopically detected [26, 4, 3, 12]. A detailed analysis of the onset of slip is not however easy to conduct from macroscopic experiments: if the length of the extrapolation of the velocity profile to zero remains small compared to the thickness of the flowing liquid, the resulting change in the relation between the pressure drop and the flow rate remains small, and may be hardly detectable. Direct investigations of the velocity at the wall thus appear as a key step in the understanding of the flow behaviour of molten polymers.

We present here a review of the work recently conducted by our group, based on direct measurements of the local velocity at the wall for one model system (polydimethylsiloxane (PDMS) against silica), in order to investigate how wall slip is influenced by polymer chains anchored to the surface, by adsorption or grafting [14, 15]. These experiments strongly support recent models [17–23], and demonstrate that, for surfaces with a weak roughness, the key parameters which govern the existence of a shear rate threshold for the onset of strong slip at the wall are the deformability of the surface-anchored polymer chains, and their degree of interdigitation and entanglement with the bulk liquid. Several regimes of wall slip have thus been identified, each regime corresponding to a particular friction law. The understanding of how the polymer surface interactions govern the structure of the surface-anchored chains and as a consequence the slip regime should open the way to the design of tailored surfaces adjusted for a particular application: efficient extrusion, controlled friction, ...

After a presentation of the two original techniques that we have developed to measure the local velocity at the polymer–wall interface, we shall briefly analyse the results obtained on layers with a weak density of strongly adsorbed chains. These results are in good qualitative agreement with the predictions of a molecular model based on the idea that the observed onset of strong slip at the wall corresponds to a dynamic decoupling between the bulk polymer and the surface chains which are deformed under the effect of the friction forces. Then, in a second step, we shall show how end-grafted layers can be formed with controlled surface densities, providing thus a far better system for checking the pertinence of this molecular model. Finally, we shall present results obtained on dense surface-anchored layers (either end grafted or strongly adsorbed) which are practically important, because they form spontaneously when a polymer melt is put into contact with an attractive wall. On such dense surface layers, we show that a transition between a weak- and a strong-slip regime do exist, but its molecular characteristics are distinct from the case of a weak dense layer. These data give evidence of collective responses of the surface-anchored chains to the flow solicitation, which will certainly have to be taken into account in theoretical descriptions.

2. Techniques for measuring the local velocity, and the experimental system

The aim of the experiments is to measure directly the velocity of a polymer melt at the solid–polymer interface, without disturbing the flow, and with a spatial resolution of the order of the radius of gyration of the polymer molecules (about 50 to 100 nm). To achieve this goal, we have developed a novel technique called ‘near-field laser velocimetry’, NFLV

for short, and another complementary technique that we call the 'volume' technique, both based on the use of fluorescent photobleachable probes as flow tracers. We shall present the principle of these two techniques, and describe the materials used in the experiments discussed in this paper.

2.1. The near-field laser velocimetry technique

This technique combines the properties of optical evanescent waves, to get the spatial resolution from the interface, and photobleaching of fluorescent molecules, which are used as non-perturbative flow tracers. Optical evanescent waves are produced when a light beam arriving from a medium with a refractive index n_1 encounters a medium of refractive index n_2, with $n_2 < n_1$. If the angle of incidence θ_i is larger than θ_c ($\theta_c = \sin^{-1}(n_2/n_1)$), total reflection occurs. Though there is no propagative wave extending into the low-index medium, energy is transferred in this forbidden medium: this is what is called the evanescent wave, characterized by an energy profile decaying exponentially in the direction normal to the interface. The decay length, or penetration depth, Λ, is related to the indices of refraction of both media and to the wavelength of the incoming light, λ_0, according to [27]

$$\Lambda = \lambda_0(4\pi\sqrt{n_1^2 \sin^2\theta_i - n_2^2})^{-1}.$$

For typical values of the indices of refraction and wavelength, the minimum value of Λ, obtained for $\theta_i = 90^\circ$, is of the order of 100 nm, which does indeed correspond to the size of a high-molecular-weight polymer molecule. The energy of the evanescent wave localized close to the interface can be used to photobleach fluorescent molecules. These photobleached probes can then act as flow tracers, by monitoring via the fluorescence intensity the way in which the flow deforms the initially created concentration profile in fluorescent probes. In classical laser velocimetry, the fluid has to be seeded with small particles which act as scatterers. To get a significant signal, the size of these particles cannot be lower than 100 nm, and thus they limit the spatial resolution and can also perturb

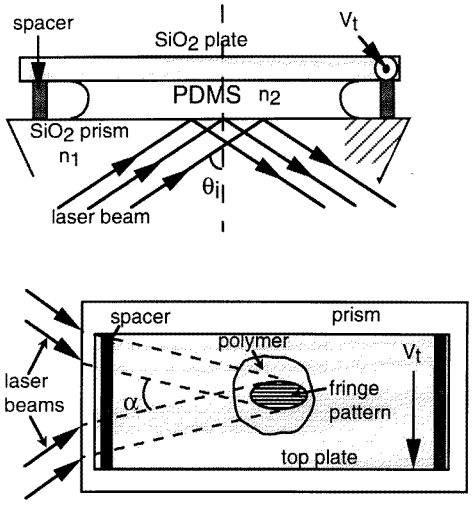

Figure 1. Schematic representations of the cell and of the laser beams used in the NFLV technique.

the flow at the interface. In the present experiments, the scattering particles commonly used in laser velocimetry are replaced by polymer chains, end labelled with fluorescent groups which can be photobleached when exposed to an intense light beam. The photobleached state has in general a lifetime much longer than the experimental time, and, for the particular fluorescent probe that we have used, it can be considered as irreversible. On the basis of the two processes described above, confinement of the excitation close to an interface by the use of evanescent waves and photobleaching of fluorescent probes, a set-up has been designed which enables the fluid velocity in a layer typically 100 nm thick at the solid–polymer interface to be determined.

The sample cell is schematically presented in figure 1. A drop of the fluorescent polymer melt ($n_2 = 1.41$) is sandwiched between the top surface of a silica prism ($n_1 = 1.46$) and a silica plate, which can be translated at a constant velocity, V_t ($0.1\ \mu\text{m s}^{-1} < V_t < 2000\ \mu\text{m s}^{-1}$) with respect to the prism, creating a simple shear flow inside the melt. The thickness of the polymer layer is fixed at $d = 8\ \mu$m by two Mylar spacers. Care is taken that the polymer drop is not in contact either with the spacers or with the edges of the prism or the plate, to avoid any perturbation of the flow. The evanescent wave is created at the prism–polymer interface by two laser beams of equal intensity which impinge on the surface with an incidence angle larger than θ_c. These two beams cross at an angle α when touching the surface, creating a fringe interference pattern in their crossing volume, with a fringe spacing of $i = \lambda_0/(2n_2 \sin(\alpha/2))$.

The experiment is performed in two steps. First the laser beams are shone at high power (about 200 mW) for 100 ms; this is the bleaching or 'writing' period. In the bright fringes some of the fluorescent molecules are bleached, creating a periodic modulation of the concentration of fluorescent molecules. Then the laser beams, attenuated by a factor of 10^3, are shone onto the interface, the silica top plate is translated, and the fluorescence intensity is recorded; this is the 'reading' period.

In order to increase the sensitivity of the detection in the reading period, a periodic modulation of the position of the fringes, at the frequency F, is turned on with an amplitude $i/2$ around the bleaching position, as proposed by Davoust *et al* [28]. The fluorescence intensity is then modulated at the frequencies F and $2F$, and these two signal components can be amplified by two lock-in amplifiers. The time dependencies of the envelopes of the F- and $2F$-signals depend on the diffusion coefficient of the labelled molecules and on the flow characteristics. If the diffusion is negligible during the duration of the reading period, and if there is neither slip at the wall nor any shear applied to the melt, the $2F$-signal has a constant amplitude, while the F-signal is zero. If a shear is applied with no slip at the interface, the concentration pattern in fluorescent probes printed in the sample during the writing period is deformed (tilting), and the $2F$-signal decreases with time while the F-signal progressively increases. Finally, if under shear there is a finite slip velocity, V_s, of the polymer melt at the prism surface, the F- and $2F$-signals show damped oscillations in phase quadrature as the printed concentration pattern passes alternately in front of the bright and dark reading fringes. The time period of the oscillations of both signals is $\tau = i/V_s$, and a simple processing of the data, fast Fourier transformation or fitting to a damped sine wave, gives V_s. An example of such an oscillating $2F$-signal is reported in figure 2. The technique obviously has some limitations. At low slip velocities the natural limiting factor is the diffusion of the fluorescent molecules, which blurs out the printed concentration pattern in fluorescent probes faster than the time constant of the oscillations in the fluorescent signal due to wall slip. If we assume a self-diffusion coefficient of the polymer molecules of $10^{-15}\ \text{m}^2\ \text{s}^{-1}$ [29], for typical experimental conditions such as those described above, and an interfringe spacing of $i = 10\ \mu$m, measurable values of V_s cannot

be lower than 1 nm s^{-1}. At high slip velocities the limitation is instrumental, and arises from the modulation technique, which fixes the upper limit at 15 μm s^{-1}.

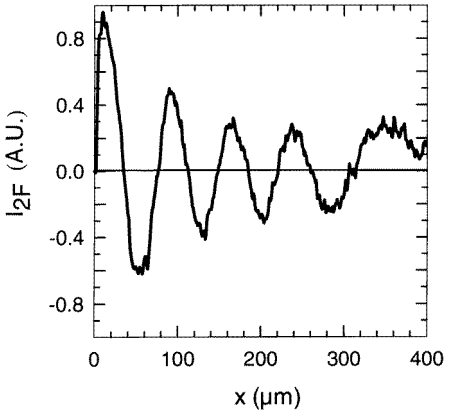

Figure 2. A typical $2F$-signal obtained by NFLV for a PDMS melt with the molecular weight 970 kg mol^{-1} flowing on a dense adsorbed layer (see section 6 for the details of the formation of such layers) obtained by incubating the clean surface of the prism in a PDMS melt with a molecular weight of 600 kg mol^{-1}. The interfringe spacing is 6.1 μm, the imposed top plate velocity is $V_t = 0.5$ μm s^{-1}, and the corresponding slip velocity is $V_s = 0.079$ μm s^{-1}.

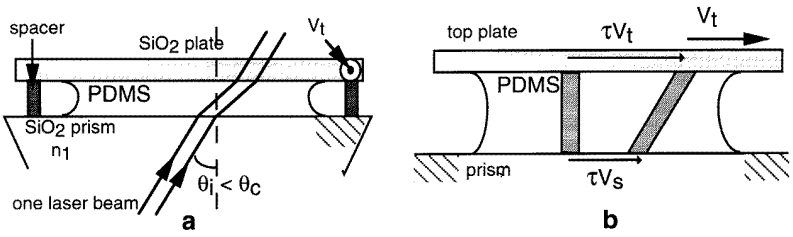

Figure 3. Schematic representations of the bleaching configuration (a) and of the deformation of the bleached line after shearing (b) in the 'volume technique'.

2.2. The 'volume technique'

To go to higher V_s-values, we have developed a second technique that we call the 'volume technique'. It still uses the photobleaching of the fluorescent molecules to trace the flow, but not the evanescent waves, and its principle is schematically presented in figure 3. During the writing phase, the light pulse of a single focused laser beam is shone through the sample, with $\theta_i < \theta_c$. A line of photobleached molecules is thus printed through the sample with a typical width of 50 μm. The entire cell is then translated in front of the laser beam, attenuated by a factor of 10^3, and the fluorescence profile is recorded. Then the shear is turned on for a time Δt. At the end of this shearing period, the fluorescence profile is recorded once more, moving the whole cell back to its starting point. The changes in position and shape of the original bleached line give information on the velocity profile (figure 3). Assuming a flow with slip at the wall, i.e. a velocity profile of the form $V(z) = V_s + \langle\dot{\gamma}\rangle z + V_t^*$, with the z-direction normal to the surface and V_t^* a possible

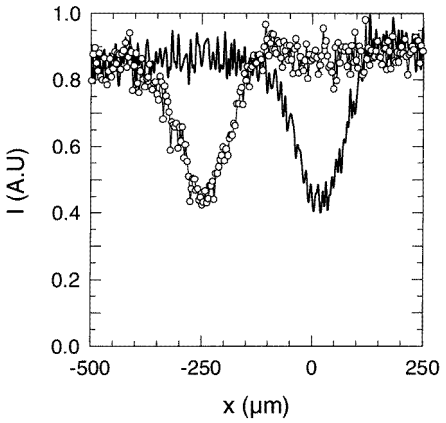

Figure 4. Typical signals obtained before (full line) and after having sheared the sample and translated it back in front of the laser beam (open dots) for the same sample as in figure 2, but now with an imposed top-plate velocity $V_t = 250\ \mu\text{m s}^{-1}$. The slip velocity deduced from the displacement of the centre of the fluorescence intensity profile is $V_s = 38\ \mu\text{m s}^{-1}$.

slip velocity at the top plate, the fluorescence intensity profile can be fitted, and the different parameters of the flow (V_s, $\dot{\gamma}$, and V_t^*) can be determined. A typical example of data obtained through this volume technique is reported in figure 4, along with the flow parameters deduced. In all of the experiments presented here, we always got $V_t^* = 0$. The volume technique also has its limitations. At low slip velocity, the diffusion of the fluorescent polymer is the limiting factor: if the broadening of the bleached line by diffusion during the duration of the measurement is larger than that due to the shear, it is impossible to fit the data in a reliable manner. With again a self-diffusion coefficient of $10^{-15}\ \text{m}^2\ \text{s}^{-1}$, V_t cannot be lower than $2\ \mu\text{m s}^{-1}$. At high slip velocities the limitation comes from the restriction in the range of possibilities of the translation mechanism of the top plate, which, in the present experiments, imposes $V_t < 1500\ \mu\text{m s}^{-1}$. It is important to notice that the ranges of V_s-values attainable by the two techniques overlap, which allows one to check the consistency of the data. A drawback of the volume technique is that the slip plane cannot be located accurately, the uncertainty being of the order of $0.8\ \mu$m. Fortunately, the cross-checking with the evanescent technique enables us to say that for all of the experiments presented here the plane of the slip is located within 100 nm of the surface.

2.3. Materials

The polymer used in the present study is α–ω OH-terminated PDMS. This polymer has a glass temperature of $-120\ ^\circ$C and is transparent. Fractions with narrow ranges of molecular weight have been obtained by means of selective precipitation techniques applied to Petrarch or Rhône–Poulenc commercial products. The characteristics of the different samples used as the bulk polymer are listed in table 1. In the following discussions, we will use the polymerization index of the bulk polymer, P, related to the weight-average molecular weight through $M_w = mP$, where $m = 0.074\ \text{kg mol}^{-1}$ is the molar mass of the monomer.

The fluorescently labelled PDMS molecules have been kindly synthesized for us by P Auroy, using a procedure described in detail in [29]. First the OH extremities of the chains of a sample with a molecular weight of 320 kg mol^{-1} were modified by reaction with an aminosilane, CH_3–O–Si–$(CH_2)_n$–NH_2, with $n = 3$ or 4; then the polymer was

Table 1. Molecular characteristics of the unlabelled PDMS.

M_w (kg mol^{-1})	M_w/M_N	M_w (kg mol^{-1})	M_w/M_N
321	1.18	785	1.22
498	1.14	962	1.27
608	1.16		

left to react with an excess of chloro-7-nitrobenzo-2-oxa-1, 3 diazole (Cl-NBD), in toluene, at room temperature for 16 hours, in the dark. After separation of the unreacted NBD, one obtains PDMS chains end labelled with NBD, with a yield which can reach 90%. As α–ω OH-terminated PDMS samples are used, most of the labelled chains bear two fluorescent probes, one at each extremity. The bulk PDMS samples analysed are all made as mixtures of labelled and unlabelled polymer (6% by weight of the labelled molecules). The labelled polymer has a maximum absorption wavelength of 468 nm, and a maximum emission wavelength of around 510 nm. The 457.9 nm line of an argon laser was used for the excitation and bleaching of the fluorescent polymer. For this wavelength, the index of refraction of the PDMS is $n_2 = 1.41$, while that of the silica prism is $n_1 = 1.46$. Thus the minimum penetration depth of the evanescent wave in the NFLV technique is 86 nm. In fact, the experiments have been performed with $\Lambda = 150$ nm, but, as both the writing and reading use the same evanescent wave, the effective thickness probed is half the penetration depth—that is, 75 nm.

To get polymer–solid interfaces with reproducible characteristics, the top plate and the prism surfaces were carefully cleaned using a two-step procedure prior to filling the cell with PDMS. First they were soaked in boiling trimethylchlorosilane (TMSCl) in a sealed reactor at 100 °C for three hours to remove most of the adsorbed PDMS. Then they were exposed to a flux of oxygen under UV irradiation [30]. Such a procedure ensures a very good cleaning (organic impurities are strongly oxidized) without any increase in the roughness of the surfaces, which stays below 8 Å r.m.s. as checked by x-ray reflectivity. In some cases, a still more efficient cleaning procedure was used, replacing the UV–ozone step by soaking in a mixture of seven volumes of pure sulphuric acid and three volumes of hydrogen peroxide in water solution (50% by weight). The surface was then rinsed with demineralized water and dried with nitrogen. Such clean silica surfaces are strongly adsorbing for PDMS, because a large density of silanol sites are available to form hydrogen bonds with the oxygen atoms of the backbone of the PDMS molecules. The top plate was used as such, and thus, for all of the experiments presented here, a dense adsorbed layer of PDMS was present on the top-plate surface. This layer ensured that slip was not visible at the top-plate–PDMS interface for shear rates at which it was well developed at the prism–polymer interface, as will be explained in section 5. On the contrary, the surface of the prism was subjected to various pre-treatments to modify it and to form different surface-anchored layers, as will be discussed for each kind of interfacial layer in the following sections.

3. Results on surfaces with a weak surface density of adsorbed chains

In figure 5, typical results obtained for the local velocity at the prism–PDMS interfaces are reported as functions of the top-plate velocity V_t. The surface of the prism has been treated by grafting on a monolayer of octadecyltrichlorosilane (OTS) molecules in order to decrease the number of PDMS molecules able to adsorb on the surface. The grafted OTS monolayer occupies most of the silanol sites of the silica surface, and the surface density

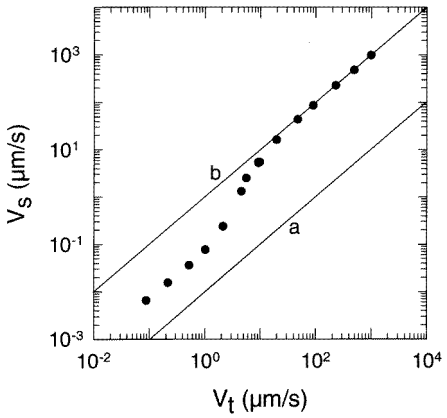

Figure 5. The variation of the slip velocity V_s versus the top-plate velocity V_t for a PDMS melt with a molecular weight of 970 kg mol^{-1} on a layer of PDMS with a molecular weight of 608 kg mol^{-1} adsorbed on an OTS monolayer deposited at the prism surface. The OTS monolayer is almost dense, characterized by an advancing contact angle for dodecane of $\theta_a = 33^\circ$. The two full lines are respectively (a) the average velocity that one would get inside the probed thickness from the surface of the prism in the case of zero velocity at the surface, $V_t \Lambda / d$, and (b) the line $V_s = V_t$. Three different slip regimes appear: a low-slip regime at low shear rates, followed by a progressive transition in which V_s increases more rapidly than proportionally to V_t, and finally a high-slip regime in which V_s becomes comparable to V_t.

of surface-anchored PDMS chains which can only adsorb in the holes of the monolayer is reduced. If the grafting conditions are such that the OTS monolayer is almost dense, only a weak density of PDMS chains can adsorb on the prism surface. The density of the OTS layer can be qualitatively characterized through the value of the advancing contact angle θ_a of the pre-treated surface with a reference liquid such as dodecane [31]. For $\theta_a > 32^\circ$, the density of adsorbed PDMS chains is on average smaller than the critical density for the mushroom regime of adsorption (surface chains just touching each other), as manifested by the thickness of the adsorbed layer, which, after rinsing off all of the unadsorbed chains and drying, is smaller than or comparable to the diameter of a PDMS monomer (10 Å). Under such conditions, the surface-anchored chains are on average independent of each other.

The data presented in figure 5 clearly display three different slip regimes at the prism–PDMS interface. At low top-plate velocities, the local velocity at the prism–polymer interface is proportional to the top-plate velocity, and larger, typically by a factor by ten, than the average velocity that one would obtain in the liquid slab for which the velocity measurement is performed (75 nm from the surface) for a zero boundary condition at the solid wall. Thus slip at the wall appears to always be present, even for the smallest shear rates investigated. Increasing the top-plate velocity, the slip velocity starts to increase more rapidly than linearly, and an onset of flow with strong slip at the wall is reached. Finally, at very high top-plate velocities, the slip velocity again becomes proportional to V_t, but with values close to V_t, and the flow is almost a plug flow.

The experiments are performed by imposing V_t and measuring V_s. If the velocity gradient is assumed to remain linear, the effective shear rate experienced by the polymer can thus easily be calculated:

$$\dot{\gamma} = \frac{V_t - V_s}{d}$$

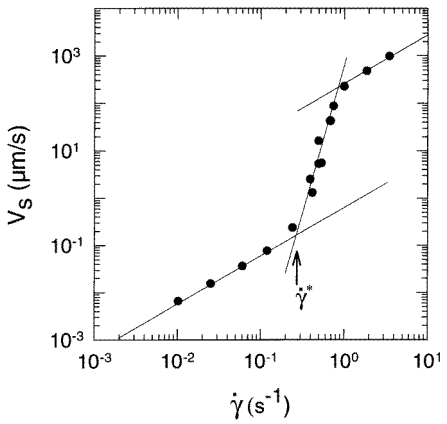

Figure 6. The same data as in figure 5, but reported in terms of the slip velocity V_s as a function of the effective shear rate experienced by the polymer, $\dot{\gamma}$. The full lines are just guides for the eye, to distinguish the three slip regimes.

with d the sample thickness. In figure 6, the data of figure 5 are reported in terms of the slip velocity, V_s, as a function of the effective shear rate experienced by the polymer, $\dot{\gamma}$. The onset of strong slip is more visible in this representation than in that of figure 5, as when V_s increases non-linearly with V_t, $\dot{\gamma}$ is no longer proportional to V_t, and tends to lock at the threshold value $\dot{\gamma}^*$.

From V_t and V_s one can also easily evaluate the length of the extrapolation of the velocity profile to zero, b, or the slip length:

$$b = \frac{V_s}{\dot{\gamma}} = \frac{V_s}{V_t - V_s} d. \tag{1}$$

b is an important characteristic of the flow. The shear stress at the wall, σ, can be written as

$$\sigma = kV_s = \eta \dot{\gamma}|_{z=0} \tag{2}$$

with η the bulk viscosity of the fluid, and k the coefficient of friction between the fluid and the surface. Combining equations (1) and (2), one gets

$$b = \eta / k. \tag{3}$$

Thus, b is inversely proportional to the coefficient of friction between the liquid and the wall. In figure 7, the data of figure 5 are reported in terms of the slip length, b, as a function of the slip velocity, V_s. Three different friction regimes are clearly visible in figure 7. At low shear rates, i.e. for small slip velocities, b appears to be independent of the slip velocity. This is a normal friction regime, with a friction force at the polymer–solid interface proportional to the local velocity V_s. b is small, of the order of a micron, implying a rather large friction coefficient. Above a critical slip velocity, V^*, b increases with V_s, following a power law $b \sim V_s^{\alpha}$ over more than three decades, with α slightly smaller than one. This is a non-trivial friction regime: a friction coefficient independent of the velocity implies a friction force which increases linearly with this local velocity; b increasing with V_s means a friction force at the interface increasing with the local velocity less rapidly than linearly. Finally, at high shear rates, a linear friction regime is recovered,

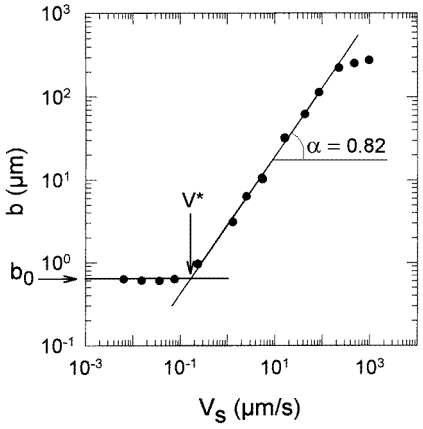

Figure 7. The same data as in figures 5 and 6, but now reported in terms of the length of the extrapolation of the velocity profile to zero, or the slip length, b, versus the slip velocity V_s. The three slip regimes are clearly visible in this representation, which allows one to more precisely characterize the polymer–wall friction (b is inversely proportional to the coefficient of friction between the polymer melt and the wall). Several parameters of the flow can be deduced from these data: the critical velocity for the onset of the non-linear intermediate-friction regime, V^*; the exponent of the power-law variation of b versus V_s in this intermediate regime; and the slip length b_0 in the weak-slip regime.

with b independent of the local velocity, but much larger than in the low-shear-rate regime, leading to a strongly reduced coefficient of friction between the fluid and the solid wall. Indeed, in this high-shear regime, the flow becomes almost a plug flow, with a slip length b much larger than the thickness of the sample, d. Varying the molecular characteristics of the PDMS melt and of the adsorbed chains, we have shown that these three different friction regimes were always present. The critical velocity, V^*, for the onset of the non-linear friction regime appeared to be highly sensitive to the polymerization indices of both the bulk and the surface chains [32], following the power laws $V^* \propto N^{-1.02\pm0.06} P^{-3.3\pm0.3}$.

4. The three slip regimes: molecular models

The first attempt to relate the velocity at the solid–polymer interface to the molecular characteristics of the polymer is due to P G de Gennes [16] for a polymer melt in contact with a smooth non-adsorbing surface. It is based on remarking that, at the interface, monomers are in contact with the solid wall, whatever the size of the macromolecules. Thus, the polymer–solid friction coefficient should be independent of the polymerization index, and identical to that of a liquid of monomers in contact with the same wall. As the usual non-slip boundary condition holds for a simple liquid, the slip length b, for the liquid of monomers, should be comparable to the size of the monomers a. Inverting equation (3), one gets a friction coefficient $k = \eta_1/a$, with η_1 the bulk viscosity of the liquid of monomers. Then using again equation (3), one obtains for the polymer case

$$b = a\frac{\eta_P}{\eta_1} \tag{4}$$

with η_P the bulk viscosity of a melt with a polymerization index P. Due to entanglements, for long enough macromolecules, η_P is much larger than η_1, and is given in the reptation

picture [33] by $\eta_P = \eta_1 P^3/N_e^2$, with N_e the average number of monomers necessary to get an entanglement. Thus, high-molecular-weight polymer melts should always display strong slip at the wall when flowing along ideal surfaces, with slip lengths in the hundreds of microns range, whatever the applied shear rate. This is not what is observed experimentally, illustrating the difficulty of getting an ideal non-adsorbing surface.

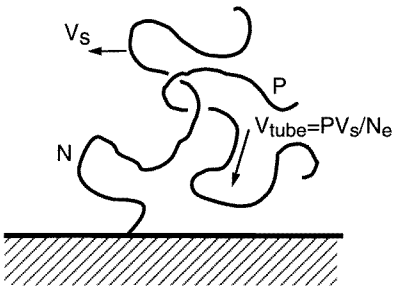

Figure 8. A schematic representation of the molecular process which allows a bulk chain, with index of polymerization P, to release its entanglement with the surface chain (with index of polymerization N), thus permitting the flow of the melt with the surface velocity V_s.

It was recognized early that the presence of a few chains strongly anchored to the solid wall should drastically affect the above picture of an ideal surface, and substantially suppress strong slip at the wall, because surface chains, if they are long enough to be entangled with the bulk polymer, lie at the origin of a strong friction at the wall [34]. In fact, the picture is more complicated, because the surface-anchored chains are not rigid objects. They can deform under the effect of the friction forces, and this deformation can strongly affect the flow behaviour. The aim of the model recently proposed by Brochard-Wyart *et al* is to describe such a process [21–23]. The situation is presented schematically in figure 8: one polymer chain (with index of polymerization N) is end grafted onto the solid wall, and entangled with the bulk polymer (chemically identical to the surface chain, and with an index of polymerization P). The only way for the bulk polymer to flow at the surface velocity V_s is for the bulk chain, during the time necessary for one bulk chain entangled with the surface chain to move parallel to the surface over a distance comparable to the average distance between entanglements, to move along its own tube, in the framework of the reptation description, over its full length, so that the entanglement is released and does not block the flow. The curvilinear velocity of the bulk chain along its tube thus needs to be $V_s P/N_e$. The friction force between the surface chain and one bulk chain entangled with it is [23]

$$f_v = \eta_1 a P \left(\frac{P}{N_e}\right)^2 V_s = \eta_P a V_s. \tag{5}$$

To compute the total friction force between one grafted chain and the bulk polymer, one needs to know the total number X of bulk chains entangled with one surface chain. This is not a trivial point: X depends on the detailed description of the entanglements and on the relative molecular weights of the surface and bulk chains, and has been discussed in detail in [23]. For 'binary' entanglements, where only two chains build up a constraint, and surface chains that are not too long ($N < N_e^2$), $X = N/N_e$, the total friction force between

the surface chain and the bulk polymer is then

$$F_v = \frac{N}{N_e} a \eta_P V_s. \tag{6}$$

For a surface with a grafting density Σ, the constraint is

$$\sigma = \frac{\Sigma}{a^2} F_v = \Sigma \frac{N}{N_e} \frac{1}{a} \eta_P V_s. \tag{7}$$

Notice that the surface density Σ is adimensional, and is related to the number of surface chains per unit surface area, ν, through $\nu = \Sigma / a^2$.

Under the effect of this friction force, each surface chain tends to elongate along the flow, taking the shape of a cigar [21] or of a trumpet in the more refined description of reference [22]. As both descriptions give the same results for the flow behaviour, we will follow here the simplest one [21]. It can be noticed that, in the binary entanglements picture, X, the number of entanglements with the melt trapped by one surface chain, remains constant when the chain is progressively deformed. X is equal to the number of trapped entanglements inside a Pincus blob [35] of the distorted chain, g/N_e, multiplied by the number of such blobs: N/g. The number of monomers inside a Pincus blob, g, decreases when the deformation of the surface chain increases, but disappears in the product. For a surface chain deformed with an average diameter D and a length Na^2/D, a restoring elastic force develops, given by the Pincus law [35]: $F_{el} = kT/D$. The balance between the elastic and viscous forces yields the diameter of the deformed surface chain:

$$D = kT \Big/ \left(\frac{N}{N_e} a \eta_P V_s \right).$$

When V_s increases, D decreases. This description holds as long as the surface and bulk chains are entangled, i.e. as long as D remains larger than the average distance between entanglements $D = N_e^{1/2} a$. This is the low-shear-rate regime of flow, characterized by a large friction due to the entanglements between the grafted chains and the bulk polymer. The wall stress, given by equation (7), increases linearly with V_s, implying a linear friction regime with a friction coefficient independent of the shear rate and of the local velocity at the wall. The corresponding slip length b is constant, equal to b_0, and given by

$$b_0 = a \frac{N_e}{\Sigma N}. \tag{8}$$

When the slip velocity becomes large enough that $D = D^*$, one enters what has been called the marginal regime [21]: the surface and bulk chains are just at the limit of being disentangled. If the slip velocity is further increased, D tends to become smaller than D^*, and the chains disentangle. If they do this, the friction force strongly decreases, and can no longer support the large elastic force associated with the deformation of the grafted chains with a diameter smaller than D^*. Thus the grafted chains tend to recoil. In the marginal regime, the diameter of the grafted chains remains locked at D^* for a range of slip velocities: the surface chains, solicited by the flow, permanently disentangle and re-entangle with the bulk polymer. This marginal regime can last as long as the frequency of that solicitation by the flow, V_s/D^*, is smaller than the inverse of the reptation time of the bulk chains, i.e. as long as the slip velocity is smaller than $V^{**} = D^*/T_{rep}(P)$. In the marginal regime, the elongation and the diameter of the surface chains are locked, and so the wall stress is

$$\sigma^* = \frac{\Sigma}{a^2} \frac{kT}{D^*}. \tag{9}$$

The critical velocity for the onset of the marginal regime is

$$V^* = \frac{kTN_e^{1/2}}{Na^2\eta_P}. \tag{10}$$

As the wall stress is independent of the local velocity, the marginal regime is a non-linear friction regime, and the coefficient of friction between the surface and the polymer fluid decreases on increasing the shear rate. The corresponding slip length b is proportional to the slip velocity:

$$b = \frac{\eta_P V_s}{\sigma^*}. \tag{11}$$

Above V^{**}, the surface chains are totally disentangled from the bulk polymer, and the friction becomes comparable to that on an ideal surface, with a slip length that is large and independent of the slip velocity. A high-slip regime is expected, which is a linear friction regime, with a weak wall friction.

The present model appears to be in quite good qualitative agreement with the experimental facts presented in figures 5 to 7. The succession of the three different slip regimes is exactly what is observed experimentally. The critical velocity for the onset of the marginal regime appears to be independent of the density of surface chains [32], while its dependencies versus the polymerization indices of either the surface or the bulk chains are observed to agree very well with equation (10) [32]. Two facts however give rise to questions. First, the effective shear rate $\dot{\gamma}$ does not really lock at a fixed value when one enters into the marginal regime (characterized by the power-law variation of b versus V_s), as seen for the V_s versus $\dot{\gamma}$ curve in figure 6, which has an S shape, and does not display a sharp jump at the shear rate threshold $\dot{\gamma}^*$. Second, the exponent of the power-law variation of b versus V_s in the marginal regime appears to be systematically slightly smaller than the predicted value 1. In order to understand the origin of these discrepancies, we have undertaken systematic experiments on a much better defined system, in which the surface chains are end grafted in a controlled way onto the silica surface. This allows us to vary and control the grafting density. We now briefly present the results obtained for this model system.

5. Results on end-grafted chains at low and moderate grafting densities

In order to form surface-anchored polymer layers in which the PDMS chains are end grafted onto the silica surface and not adsorbed by any of their monomers, one needs to modify the silica surface to suppress all of the silanol sites of the surface which are potential adsorption sites for the PDMS molecules. This modification has to be chosen in such a way that the possibility of reacting one extremity of each of the PDMS chains to form a covalent bond is maintained. We have elaborated a procedure for doing this, which has been described in detail elsewhere [36]. We recall here the main steps and results, to explain how the grafting density and the structure of these layers are controlled. We first synthesized chlorooctamethyl-tetrasiloxane, and grafted a self-assembled monolayer of this short PDMS oligomer on the surface of the prism. This surface thus becomes a carpet of SiH extremities. Good quality of the self-assembled monolayer is essential for the further control of the grafted PDMS layer [36]. On this SiH carpet, the vinyl ends of the monofunctional PDMS chains (that we have anionically synthesized) were grafted using a platinum-catalysed hydrosililation reaction. The concentration of PDMS chains in the reaction bath (in solution in octane, at a volume fraction ϕ) controls the number of chains

which can access the surface, and, as the grafting reaction is fast, this fixes the grafting density. The dry thickness of the grafted layer, h, after rinsing off all of the unreacted chains, measured by x-ray reflectivity, is observed to be proportional to $N^{1/2}\Phi^{7/8}$ [36]. The surface density of the grafted chains Σ can easily be deduced from this dry thickness:

$$\Sigma = \frac{h}{aN} = N^{1/2}\phi^{7/8}. \tag{12}$$

The above-described procedure leads to controlled layers with adjustable surface densities, in the range 3×10^{-3} to 4×10^{-2}, always larger than the overlap threshold $\Sigma^* = 1/N \sim 7.7 \times 10^{-4}$ for the particular molecular weight used to form the grafted layer (96 kg mol^{-1}).

The flow behaviour of different PDMS melts (with molecular weight in the range 400 kg mol^{-1} to 970 kg mol^{-1} and polydispersity index $I < 1.2$) has been investigated for layers of grafted chains with a molecular weight of 96 kg mol^{-1} at various grafting densities. Three different regimes of response of the samples to shear were always observed [37]: a weak-slip regime at low shear rates, characterized by an extrapolation length of the velocity profile to zero, b_0, in the micron range, and independent of the slip velocity (the linear friction regime with high polymer–wall friction); then, above a critical slip velocity V^*, a marginal regime, over three decades in slip velocity, in which the slip length b increases linearly with V_s (the non-linear friction regime); and finally, a high-slip regime at large shear rates, in which b again becomes independent of V_s, but now has a large value, typically 30 μm, much larger than the size of the grafted chains. This is qualitatively very similar to what has been observed for the weakly dense adsorbed layers, described in section 2. Several features however are clearly different: as reported in [37], inside the marginal regime, the shear rate strictly locks at the threshold value $\dot{\gamma}^*$, and the V_s versus $\dot{\gamma}$ curves appear vertical inside this regime (while they had a S shape for the adsorbed surface chains). At the same time, the exponent of the power-law variation of b versus V_s is always 1 when there are grafted chains on the surface. These features, which are in full quantitative agreement with the predictions of the molecular model described in section 3, lead us to interpret both the S shape of the V_s versus $\dot{\gamma}$ curve, and the observed small exponent for the b versus V_s law, in the marginal regime, in the case of adsorbed chains, as a polydispersity effect. Indeed, on the OTS-modified silica, the chains can adsorb via any of their monomers, and form tails or loops which entangle with the bulk melt. Because the OTS layer is almost dense, we think that the probability of forming loops should be rather small (loop formation necessitates several adsorption sites being closer to each other than the radius of the adsorbed chains). If tails are the most probable structures which entangle with the bulk polymer, they obviously do not all have the same length. The effect of polydispersity has been briefly discussed in [21]. The result is an onset of the marginal regime which is that of the longest chains, above which b is no longer independent of V_s. But the shorter chains of the distribution enter progressively into their marginal regime as V_s increases. The chains which are not yet marginal contribute to a surface stress increasing linearly with V_s, while those that are already marginal contribute to a surface stress locked at its threshold value. The result of the polydispersity is thus a smoothing of the V_s versus $\dot{\gamma}$ curve, while an abrupt threshold appears as soon as the polydispersity is kept small. At the same time, the exponent of the power-law variation of b versus V_s can no longer be 1 as soon as the stress is not strictly locked, as b, V_s, and $\dot{\gamma}$ are related through equation (1). In the light of the experiments performed on grafted chains, we thus think that the deviations first observed between the molecular model and the experimental results obtained on adsorbed chains at low surface densities do not in fact force one to question the model, but rather can be accounted for within the framework of this model if one takes into account the polydispersity of the tails

of the adsorbed chains. As a consequence, the friction behaviour of a flowing melt appears to be a quite sensitive tool with which to investigate surface-anchored polymer layers.

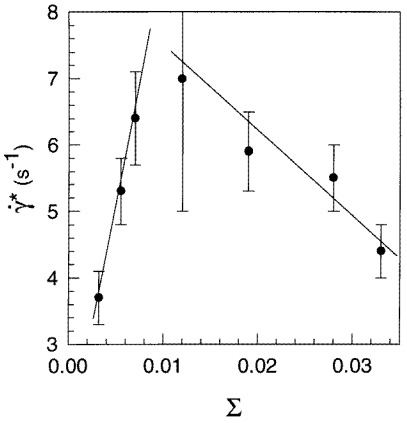

Figure 9. The evolution of the shear rate threshold for the onset of the marginal regime, $\dot{\gamma}^*$, as a function of the grafting density in the surface layer, Σ, for a PDMS melt with a molecular weight of 970 kg mol^{-1} flowing on end-grafted chains with a molecular weight of 96 kg mol^{-1}. The first, linearly increasing branch of the curve corresponds to surface chains which behave independently of each other, while the second, decreasing part is an indication of the fact that at high surface densities, the surface chains respond collectively to the flow solicitation.

A second interesting area of the experiments performed on the grafted layers is that, by controlling the surface density, the molecular model of [21] can be further tested. In figure 9, the evolution of the shear rate threshold for the onset of the marginal regime, $\dot{\gamma}^*$, is reported as a function of the grafting density, Σ, for a PDMS melt with a molecular weight of 970 kg mol^{-1} on the grafted layers already described. Figure 9 clearly shows two very different behaviours: $\dot{\gamma}^*$ first increases linearly with Σ and then decreases at large surface densities. As $\dot{\gamma}$ is directly related to the surface stress, a $\dot{\gamma}^*$-value depending linearly on Σ means that, at the onset of the marginal regime, the surface chains act independently of each other, and enter into their marginal regime at a fixed drag force per chain. On the other hand, a $\dot{\gamma}^*$ decreasing with Σ is a clear indication of a new regime in which the surface chains are no longer independent of each other in their response to the flow. As already discussed in [37], it is surprising to see that, for all of the data reported for the linearly increasing regime of figure 9, the corresponding slip length at low shear, b_0, is observed to be independent of Σ. This is not what is predicted by equation (8). The data reported for that first linearly increasing part of the curve in figure 9 manifest a new and non-trivial regime for the dynamic coupling between the surface layer and the bulk polymer, which has been predicted by C Gay *et al* [23]. If one starts from very low densities of grafted chains and progressively increases Σ, the number of bulk chains entangled with the surface chains progressively increases, up to the maximum value of the surface density for bulk chains, $\Sigma_b = P^{-1/2}$. Then the surface layer can no longer trap more bulk chains. The slip length then is expected to become independent of Σ, and given by $b_0 = aP^{1/2}$. This should in any case not affect the Σ dependence of $\dot{\gamma}^*$, because the surface chains all need to be elongated with a diameter equal to D^* to enter into their marginal regime, leading to $\eta_P\dot{\gamma}^* = \Sigma kT/D^*$, as long as the surface chains remain independent of each other during deformation under the

effect of the friction force. At this stage, the experimental data obtained on the PDMS–silica system fully agree with the molecular model developed by de Gennes and co-workers. The observed progressive transition between a weak-slip regime at low shear rates and a strong-slip regime at high shear is the signature of a dynamic decoupling between surface-anchored chains and the bulk polymer. The transition is progressive, and is characterized by what has been called the marginal regime, because over a large range of slip velocities (more than two decades in all of the experiments presented here) the surface chains remain just at the limit of being disentangled from the melt. One has to go to high shear rates to be able to fully stretch the surface chains and to observe strong slip similar to that expected for ideal surfaces. It has been argued that the onset of strong slip at the wall could also be due to the desorption of surface-adsorbed chains [38]. We think that the observed wide marginal regime, and the very similar behaviours observed for adsorbed and end-grafted surface chains, strongly support a mechanism for the onset of strong slip at the wall associated with the elongation and the progressive disentanglement of the surface and the bulk chains, and rule out an onset of strong slip associated with desorption of the surface chains, for the particular system that we have investigated. In its present state, the model developed by de Gennes *et al* deals with surface chains with rather weak surface densities (with an independent response to the flow). In figure 9, evidence of other regimes at high surface densities is shown. This is of great practical importance, as when a polymer melt is put into contact with an attractive wall, dense surface-anchored layers form spontaneously. We wish to present now an investigation on how the flow behaviour is affected by the molecular parameters of the system on such dense surface-anchored layers.

Table 2. Characteristics of the PDMS melts used to form dense surface-anchored layers at the prism surface.

M_w (kg mol^{-1})	M_w/M_N	M_w (kg mol^{-1})	M_w/M_N
37	1.14	293	1.14
53	1.14	402	1.14
105	1.12	475	1.16
193	1.20	610	1.16

6. Results on dense surface-anchored layers

Irreversibly adsorbed PDMS layers can be formed on the clean silica surface of a prism, using a method described for silicon wafers [39]. The surface of the prism needs first to have any trace of PDMS cleaned off by the procedure described in section 2.3. It is then put into contact with a solution of PDMS in octane with a volume fraction ϕ, in a sealed reactor, at 120 °C for one night. After rinsing off the unadsorbed polymer and drying, the thickness of the dry layer, h, is characterized by x-ray reflectivity. Similarly to what has already been said for grafted layers, all of the chains which have access to the surface immediately after the cell is rapidly filled find adsorption sites and fix onto the silica. Thus h is observed to be equal to $aN^{1/2}\phi^{7/8}$ [39], with $a \sim 0.5$ nm, very close to the monomer size. As in the dry state all of the monomers forming the layer are closely packed, the surface density of chains in the surface layer is given by equation (12). It is worthwhile mentioning at this stage that equation (12) does not tell us anything about the structure of the surface layer, and is the same for grafted and adsorbed layers. This simply arises from the fact that all

of the chains in the reaction bath located at a distance from the wall comparable to their radius are able to bind to the surface.

In table 2, we have collected together the molecular characteristics of the PDMS samples used to form adsorbed layers on the surface of the prism. They were all of dihydroxy-terminated PDMS, obtained by fractionation of a Petrarch 800 000 cst batch.

In the following, the data will be discussed in terms of the polymerization index of the chains in the surface layer, N, related to their weight-average molecular weight through $M_w = mN$ ($m = 0.074$ kg mol^{-1} is the molar mass of the monomer).

The internal structure of these adsorbed layers has been investigated in detail, including an analysis of their swollen thickness in good solvents, both with modified-tip AFM techniques [40] and by neutron reflectivity [41]. They have been observed to be well described in terms of Guiselin pseudo-brushes [42].

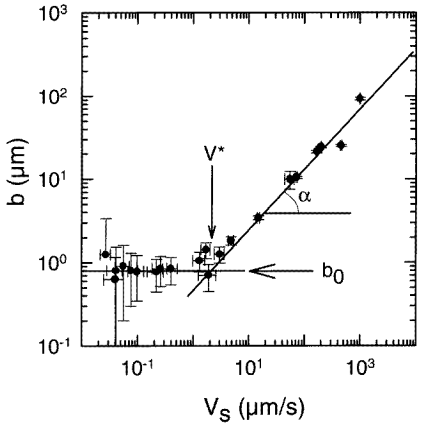

Figure 10. b versus V_s for a PDMS melt with a molecular weight of 970 kg mol^{-1} flowing on a pseudo-brush with a molecular weight of 193 kg mol^{-1} and a surface density of $\Sigma = 0.0071$.

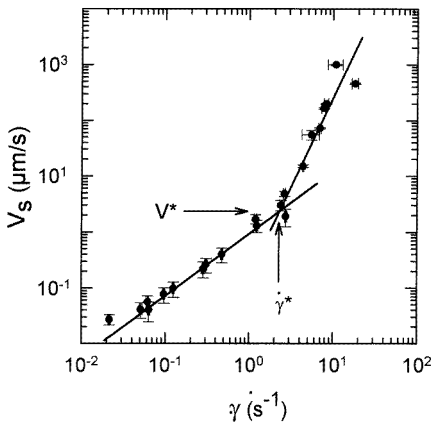

Figure 11. This same data as in figure 10, but reported in terms of the slip velocity V_s as a function of the effective shear rate experienced by the polymer, $\dot{\gamma}$.

The flow behaviour of different PDMS melts (molecular weights in the range 300 kg mol^{-1} to 970 kg mol^{-1}) has been investigated as functions of the surface density and of the molecular weights in the surface layer. In all cases, a slip transition is observed when the slip velocity crosses the critical value V^*, as shown in figures 10 and 11. On the two sides of the transition the responses of the sample to the shear stress are different. For small slip velocities $V_s < V^*$, the slip length b has a value b_0 which is independent of V_s. For $V_s > V^*$, b takes on a form of a power law in V_s, $b \sim V_s^{\alpha}$, with an average value of the exponent α over all of the experiments performed of $\alpha = 1 \pm 0.2$, and values ranging from 0.73 to 1.40. In terms of the shear rate, $\dot{\gamma}$ appears to be linear in V_s for $V_s < V^*$. When V_s becomes larger than V^*, $\dot{\gamma}$ is almost locked, and increases very slowly with V_s:

$$\dot{\gamma} = \frac{V_s}{b} \propto V_s^{1-\alpha}. \tag{13}$$

In the present experiments, b_0 and V^* are determined directly from the experimental data, and the value of the shear rate at the transition, $\dot{\gamma}^*$, is deduced through the relation $\dot{\gamma}^* = V^*/b_0$.

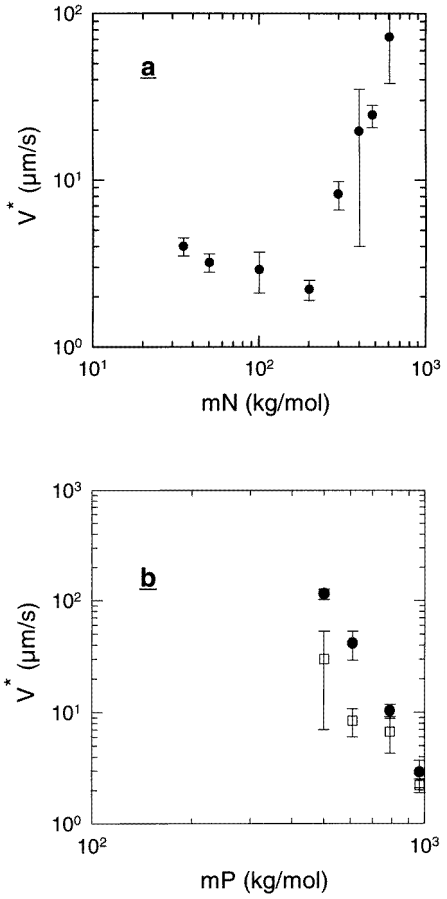

Figure 12. The evolution of the critical velocity V^* with the molecular weights of both the adsorbed surface layer and the flowing melt. The pseudo-brushes have been formed from the melt, and are thus at their maximum density for each molecular weight. In (a), V^* is reported as a function of the pseudo-brush molecular weight mN for a flowing melt with a molecular weight of 970 kg mol^{-1}. In (b), the variation of V^* as a function of the molecular weights of the flowing melt are analysed for the two different regimes identified in (a): filled circles: $mN = 105$ kg mol^{-1} and $\Sigma = 0.027$; squares: $mN = 193$ kg mol^{-1} and $\Sigma = 0.019$.

We have investigated the influence of the polymerization index of the adsorbed chains, N, on the parameters of the transition, for a flowing PDMS melt with a molecular weight of 970 kg mol^{-1}. The data for pseudo-brushes made from a melt ($\phi = 1$) are reported in figure 12. Notice that, as $\phi = 1$, the surface density is not a constant for these data, but varies as $N^{1/2}$. V^* is observed to be a non-monotonic function of N. It first slowly decreases with N up to $N = 2600$ (the molecular weight of the pseudo-brush is 193 kg mol^{-1}). For larger molecular weights, V^* increases with N, following the power law

$$V^* \propto N^{3.0\pm0.2}. \tag{14}$$

The slip length b is also sensitive to N. In the weak-shear-rates regime, b_0 seems to show a weak minimum when N is increased, but the results are difficult to interpret, due to the relatively large uncertainty in the determination of b_0. Above V^*, the exponent α is different

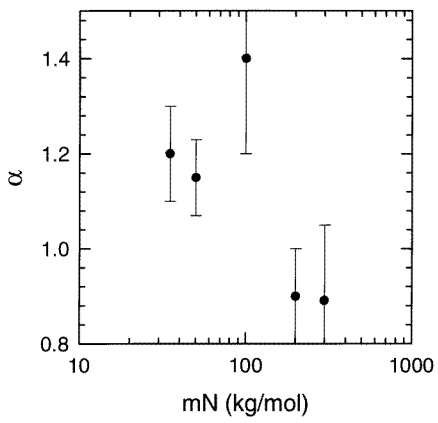

Figure 13. The dependence of the exponent of the power-law variation of the slip length versus the slip velocity, α, inside the marginal regime, versus the molecular weight inside the pseudo-brush. The molecular weight of the flowing PDMS melt is 970 kg mol^{-1}.

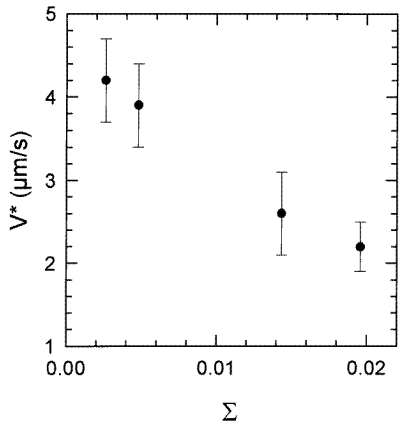

Figure 14. The influence of the surface density inside the pseudo-brush, Σ, on the critical velocity for the onset of the marginal regime, V^*, for $mP =$ 970 kg mol^{-1} and $mN = 193$ kg mol^{-1}.

in the two regimes of variation of V^* versus N, as shown in figure 13: it is of the order of 1.2 for $N < 2600$, and smaller than or equal to 0.9 for larger N-values. V^* is also highly sensitive to the molecular weight of the flowing melt, for the two regimes $N < 2600$ and $N > 2600$. Power laws are observed, with, respectively, an exponent of -5.4 ± 0.2 for small N and -3.4 ± 0.5 for larger N.

Finally, we have investigated the influence of the surface density in the pseudo-brush, Σ, on V^* for a melt with a molecular weight of 970 kg mol^{-1}, and pseudo-brushes with $N = 2600$. The results are reported in figure 14: V^* is a decreasing function of Σ. We have no model of the mechanisms of the dynamic decoupling between the polymer melt and the pseudo-brush at large surface densities. And, indeed, all of the dependencies versus the molecular parameters of the system appear to strongly differ from what has been observed in the weak-surface-density limit, either for the adsorbed or for the grafted chains. Qualitatively, anyway, the transition between a weak- and a strong-slip regime appears very similar to what has been observed in the case of independent surface chains. In particular, the transition towards a strong-slip regime is progressive, and is characterized by power-law dependencies of the slip length versus the slip velocity, over several decades. It is thus tempting to assume that the underlying mechanism is the same as that described in section 3. This picture allows one to qualitatively understand the data reported above. For the pseudo-brush, the difficult problem is that of identifying the interacting chains, i.e. of gaining a knowledge of the degree of interpenetration between the melt and the adsorbed chains, and of how this degree of interpenetration is affected by the flow. The degree of interpenetration of a grafted brush and a melt has been investigated in detail theoretically under static conditions [43–45]. The tendency is that large molecular weight melts should be expelled from the brush, and that this expulsion is more efficient and occurs for smaller molecular weights when the surface density is increased. Similar trends are expected for the pseudo-brushes [45], but it has been shown experimentally through neutron reflectivity data that pseudo-brushes were penetrated to a greater degree by a melt than the brushes with the same molecular weight and surface density [46]. For the experiments performed

with $\phi = 1$, as the molecular weight of the flowing melt is always much larger than that of the pseudo-brush, we expect a low degree of interpenetration. However, at low shear rates, such pseudo-brushes develop a friction force against a melt comparable to that obtained on grafted layers with moderate surface densities (b_0 has comparable values). This may indicate that only a weak interpenetration with a large number of surface chains can develop a large friction. For the experiments performed varying Σ at fixed molecular weights in both the surface layer and the melt, one can expect an increasing degree of interpenetration as Σ decreases. This can qualitatively explain the fact that the observed V^* is a decreasing function of Σ. The influence of N can also partly be understood as being due to a variation of the degree of interpenetration: at low N-values, a given melt is expelled to a greater degree from the surface layer than for larger N, closer to P. For $N \ll P$, one can expect that only the longest loops and tails in the pseudo-brush will interact dynamically with the melt. Their surface density varies as $N^{-1/2}$ [42], i.e. does not vary much in the range 473–2600 (only by a factor by 2). As a consequence, V^* should not be strongly affected by N, as is observed in figure 14. For higher molecular weights of the surface layer, the degree of interpenetration should increase, the melt interacting dynamically with deeper and deeper loops, leading to V^*-values rapidly increasing with N.

It is also interesting to compare the wall slip behaviour observed for pseudo-brushes to that obtained for grafted brushes with similar characteristics. The main important difference is that, in the case of grafted brushes, the shear rate at the transition is locked at its transition value $\dot{\gamma}^*$ throughout the marginal state, while for the pseudo-brushes, $\dot{\gamma}$ goes on increasing slowly inside the marginal regime. As for the weakly dense surface layers, we think that this reflects the polydispersity of the loops and tails. The values of the parameters of the transition, b_0 and V^*, can also be compared. The results are summarized in table 3 for systems with similar molecular parameters.

Table 3. Comparison of the dynamic parameters of the wall slip, b_0 and V^*, for a PDMS of molecular weight 970 kg mol^{-1} on grafted and adsorbed surface layers with comparable molecular weights and surface densities.

M_w (kg mol^{-1}) inside the surface layer	Σ	Pseudo-brush		Brush	
		b_0 (μm)	V^* (μm s^{-1})	b_0 (μm)	V^* (μm s^{-1})
100	0.027	0.44 ± 0.02	3.2 ± 0.4		
96	0.0028			1.9 ± 0.3	10.5 ± 1.0
193	0.019	0.51 ± 0.03	2.2 ± 0.3		
200				1.8 ± 0.2	9.0 ± 0.9

b_0 appears to be smaller for the pseudo-brush than for the equivalent brush, by a factor of 4. This means that the friction of the melt on a pseudo-brush is higher than that on a brush. V^* is also smaller in the case of the pseudo-brush, by a factor of 3 to 4, with the result that it is easier to reach the marginal state for a melt against a pseudo-brush than with a brush. These two observations are signatures of the same fact: at a given slip velocity, the friction against the pseudo-brush is larger than that against the equivalent brush. The pseudo-brush will be more deformed, and will reach its threshold for full disentanglement more rapidly. This is consistent with the idea that a pseudo-brush is more easily penetrated by a melt than the equivalent brush, i.e. that the polydispersity of the loops and tails favours interpenetration [46].

7. Conclusion

We have presented a series of experiments aimed at characterizing the interfacial boundary conditions for the velocity of a sheared polymer melt on various surface-anchored polymer layers. This was feasible thanks to two velocimetry techniques that we have developed, and which give direct access to the flow velocity in the immediate vicinity of a solid wall (typically in a slab with a thickness of 100 nm from the wall). By controlling the surface chemistry of the solid surface (silica), we have been able to form different surface-anchored polydimethylsiloxane layers, with controlled surface densities, structures, and molecular weights.

On such decorated surfaces, a high-molecular-weight polydimethylsiloxane melt flows, displaying systematically a succession of three different friction regimes. At low shear rates, weak slip at the wall is observed, with a friction coefficient independent of the slip velocity, due to entanglements between the surface-anchored chains and the bulk polymer. On increasing the shear rate, a critical slip velocity V^* is attained above which a non-linear friction regime appears. This is characterized by power-law dependencies for the coefficient of friction between the fluid and the surface. This friction coefficient decreases with increasing shear rates, due to a progressive dynamic decoupling of the surface and the bulk chains. Finally, at high shear rates, the surface chains are totally disentangled from the melt, and a linear friction regime is recovered with a small friction coefficient analogous to that expected for ideal surfaces: the slip velocity is large, and the flow is close to a plug flow. The characteristic parameters of this transition from weak to strong slip at the wall appear to be highly sensitive to the molecular parameters of the system: the molecular weights of both the surface and bulk chains, and the surface densities of the anchored chains. They are also affected by the molecular organization inside the surface layer, because such organization fixes both the degree of interpenetration of the bulk and surface chains, and the deformability of these latter under the effect of the friction forces. For all of the regimes in which the surface chains are independent of each other, we have obtained a full agreement between the experimental results and a model which describes in detail the dynamic decoupling of the surface and bulk chains. For larger surface densities, the results show evidence of collective responses of the surface layer to the flow solicitation. The variations of the critical slip velocity V^* can then qualitatively be understood as being mainly driven by the degree of interdigitation of the surface and bulk chains, which is a non-trivial function of the surface densities and molecular weights. On these dense surface layers, the internal structure inside the surface layer has a marked effect on the level of friction, and an adsorbed layer displays a friction coefficient for a given melt four times larger than that for the equivalent grafted layer. These experiments open the way to a full understanding of the dynamical coupling between a surface-anchored polymer layer and a polymer melt, and should allow the design of surfaces with adjusted friction properties.

References

[1] Ramamurthy A V 1986 *J. Rheol.* **30** 337
[2] Benbow J J and Lamb P 1963 *SPE Trans.* **3** 7
[3] Vinogradov G V, Protasov V P and Dreval V E 1984 *Rheol. Acta* **23** 46
[4] El Kissi N and Piau J M 1990 *J. Non-Newtonian Fluid Mech.* **37** 55
[5] Kalika D S and Denn M M 1987 *J. Rheol.* **31** 815
[6] Funatsu K and Sato M 1984 *Adv. Rheol. (Mexico)* **4** 465
[7] Knappe W and Krumböck E 1984 *Adv. Rheol. (Mexico)* **3** 417
[8] De Smedt C and Nam S 1987 *Plastic Rubber Process Appl.* **8** 11

[9] Hatzikiriakos S G and Delay J M 1991 *J. Rheol.* **35** 497
[10] Burton R H, Folkes M J, Narh K A and Keller A 1983 *J. Mater. Sci.* **18** 315
[11] Galt J and Maxwell B 1964 *Modern Plastics* (New York: McGraw-Hill)
[12] Atwood B T and Schowalter W R 1989 *Rheol. Acta* **28** 134
[13] Migler K B, Hervet H and Léger L 1993 *Phys. Rev. Lett.* **70** 287
[14] Migler K B, Massey G, Hervet H and Léger L 1994 *J. Phys.: Condens. Matter* **6** A301
[15] Léger L, Hervet H, Marciano Y, Deruelle M and Massey G 1995 *Israel J. Chem.* **35** 65
[16] de Gennes P G 1979 *C. R. Acad. Sci., Paris* B **288** 219
[17] Leonov A I 1984 *Rheol. Acta* **23** 591
[18] Chernyak Y B and Leonov A I 1986 *Wear* **108** 105
[19] Lau H C and Schowalter W R 1986 *J. Rheol.* **30** 193
[20] Leonov A I 1990 *Wear* **141** 137
[21] Brochard-Wyart F and de Gennes P G 1992 *Langmuir* **8** 3033
[22] Ajdari A, Brochard-Wyart F, Gay C, de Gennes P G and Viovy J L 1995 *J. Physique* II **5** 491
Ajdari A, Brochard-Wyart F, de Gennes P G, Leibler L, Viovy J L and Rubinstein M 1994 *Physica* A **204** 17
[23] Brochard-Wyart F, Gay C and de Gennes P G 1996 *Macromolecules* **29** 377
[24] Petrie C J S and Denn M M 1976 *AIChE J.* **22** 209
[25] Piau J M, El Kissi N and Tremblay B 1990 *J. Non-Newtonian Fluid Mech.* **34** 145
[26] Benbow J J and Lamb P 1963 *SPE Trans.* **3** 7
[27] Born M and Wolf E 1964 *Principles of Optics* (New York: MacMillan)
[28] Davoust J, Devaux P and Léger L 1982 *EMBO J.* **1** 1233
[29] Léger L, Hervet H, Auroy P, Boucher E and Massey G 1996 *Rheology for Polymer Processing* ed J M Piau and J F Agassant (New York: Elsevier) p 1
[30] Vig J R 1987 *Treatise on Clean Surfaces Technology* ed K L Millal (New York: Plenum)
[31] Silberzan P and Léger L 1991 *Phys. Rev. Lett.* **66** 185
Silberzan P, Léger L, Aussérré D and Benattar J J 1991 *Langmuir* **7** 1647
[32] Massey G, Hervet H and Léger L 1997 *Europhys. Lett.* submitted
[33] de Gennes P G 1979 *Scaling Concepts in Polymer Physics* (Ithaca, NY: Cornell University Press) p 223
[34] Brochard-Wyart F, de Gennes P G and Pincus P 1992 *C. R. Acad. Sci., Paris* **314** 873
[35] Pincus P 1976 *Macromolecules* **9** 386
[36] Folkers J P, Deruelle M, Durliat E, Marzolin C, Hervet H and Léger L 1997 *Macromolecules* submitted
[37] Durliat E, Hervet H and Léger L 1997 *Europhys. Lett.* **38** 383
[38] Woo Y W and Wang S Q 1996 *Phys. Rev. Lett.* **76** 467
[39] Deruelle M, Ober R, Hervet H and Léger L 1997 *Macromolecules* submitted
[40] Deruelle M, Ondarçuhu T and Léger L 1997 *Langmuir* submitted
[41] Marzolin C, Hervet H, Folkers J P and Léger L 1997 *Macromolecules* submitted
[42] Guiselin O 1992 *Europhys. Lett.* **17** 225
[43] de Gennes P G 1976 *J. Physique* **37** 1443
de Gennes P G 1980 *Macromolecules* **13** 1069
[44] Aubouy M and Raphaël E 1994 *Macromolecules* **27** 5182
[45] Ligoure C 1996 *Macromolecules* **29** 5459
[46] Marzolin C, Hervet H and Léger L 1997 *Macromolecules* submitted